SCIENTIFIC REPORTS

OPEN

SUBJECT AREAS:
CHEMISTRY
MATERIALS CHEMISTRY
NANOSCIENCE AND TECHNOLOGY
ELECTRONIC DEVICES

Received
2 July 2012

Accepted
12 September 2012

Published
3 October 2012

Correspondence and requests for materials should be addressed to X.Z. (xbzhang@ciac.jl.cn)

General and Controllable Synthesis Strategy of Metal Oxide/TiO_2 Hierarchical Heterostructures with Improved Lithium-Ion Battery Performance

Hengguo Wang[1], Delong Ma[1,2], Xiaolei Huang[1,3], Yun Huang[1,2] & Xinbo Zhang[1]

[1]State Key Laboratory of Rare Earth Resource Utilization, Changchun Institute of Applied Chemistry, Chinese Academy of Sciences, 130022 Changchun, China, [2]Key Laboratory of Automobile Materials, Ministry of Education, and School of Materials Science and Engineering, Jilin University, Changchun 130012, China, [3]Graduate University of Chinese Academy of Sciences, Beijing 100049, P. R. China.

We demonstrate a simple, efficient, yet versatile strategy for the synthesis of novel hierarchical heterostructures composed of TiO_2 nanofiber stem and various metal oxides (MOs) secondary nanostructures, including Co_3O_4, Fe_2O_3, Fe_3O_4, and CuO, by advantageously combining the versatility of the electrospinning technique and hydrothermal growth method, for which the controllable formation process and possible formation mechanism are also investigated. Moreover, as a proof-of-concept demonstration of the functional properties of these hierarchical heterostructures, the Co_3O_4/TiO_2 hierarchical heterostructures are investigated as the lithium-ion batteries (LIBs) anode materials for the first time, which not only delivers a high reversible capacity of 632.5 mAh g^{-1} and 95.3% capacity retention over 480 cycles, but also shows excellent rate capability with respect to the pristine TiO_2 nanofibers. The synergetic effect between Co_3O_4 and TiO_2 as well as the unique feature of hierarchical heterostructures are probably responsible for the enhanced electrochemical performance.

Growth of functional semiconductor oxides with controllable hierarchical heterostructures has attracted tremendous attention because diverse properties can be integrated by tailoring the morphology, composition, and assembling organization of the primary nanobuilding blocks. Specifically, novel hierarchical heterostructures, in which the major 1D cores and branches consist of different materials, are more attactive in many nanoscale photonic and electron-optical device applications. Especially, to serve as materials for lithium-ion batteries (LIBs), the hierarchical heterostructures not only integrate the diverse properties from the different building blocks, but also exhibit intriguing properties by taking advantage of both the nanometer-size effects and the high stability of the secondary-structure assemblies[1–6]. For instance, epitaxial growth of branched α-Fe_2O_3/SnO_2 nano heterostructures could improve LIB performance due to the synergetic effect exerted by SnO_2 and α-Fe_2O_3 as well as the unique branched structure[5]. Furthermore, a novel high performance cathode material for LIBs has been developed by coating V_2O_5 on SnO_2 nanowires, utilizing the better conductivity of SnO_2 nanowires and the short diffusion distance of the thin V_2O_5 layer[6]. Notwithstanding these advances, it is still of great challenge to develop a general approach with the characteristics of low cost, low growth temperature, environmental friendliness, process simplicity, and high yield to synthesize a control of size, dimension, and composition of the building blocks of hierarchical heterostructures in an expected manner.

TiO_2, as an important functional material, has numerous applications as photocatalysis, electronic devices, conversion devices as well as promising electrode material due to its attractive advantages of high abundance, low cost, better safety, and environmental friendliness[7–13]. Furthermore, the special structural characteristics and surface activity, together with the very low volume change during Li^+ insertion/desertion (3–4%), intrinsically endows TiO_2 good structural stability and long cycle life[14–17]. Nevertheless, the main weaknesses of TiO_2 as anode materials for LIBs lie in the low theoretical capacity (168 mAh g^{-1}, even lower than that of commercial graphite

~372 mAh g^{-1}) and the poor rate capability of TiO_2 electrodes. Recently, different strategies, such as constructing one dimensional (1D) TiO_2 nanostructures (nanorod, nanofiber, nanotube, and core-shell nanowire)[18–21] and coating or mixing with more conductive materials, such as carbonaceous materials[22–24], noble metals (Au, Ag etc)[25,26], and RuO_2[27], and/or doping with foreign atoms[20,28] have been developed to overcome the ionic and electronic transport limitations and improve the rate capability of TiO_2-based anodes. However the strategies mentioned above still suffer from disadvantages such as high cost, complicated production procedure, and to add insult to injury decrease the capacity of TiO_2, because these coating materials are not very active materials for reversible lithium storage. Therefore, it is urgently important to develop new strategies that can coat the active materials with high capacity and conductivity on the surface of TiO_2 nanostructures. On the other hand, as a new class of promising anode materials for LIBs, transition-metal oxides (MOs) have shown desirable property of higher theoretical capacities (700–1000 mAh g^{-1}, which is much higher than that of commercial graphite and TiO_2)[29–34]. However, an intrinsically drastic volume change during lithiation/delithiation process gives rise to pulverization that may break the electrical contact pathways in the MOs electrodes, thus leading to a rapid decay in capacity and limiting the practical use. Therefore, developing new synthetic strategies to fabricate high-performance MOs electrode materials with both large reversible capacity and long cycle life are highly desirable but still very challenging.

Stimulated by the above concerns, we envision building up an integrated smart architecture, in which structural features and electroactivities of each component are fully manifested, the interface/chemical distributions are homogeneous at a nanoscale and a fast ion and electron transfer is guaranteed. Herein, we propose and realize a facile, effective, and general strategy for preparing MOs/TiO_2 hierarchical heterostructures by advantageously combining the electrospinning technique with the hydrothermal method, which holds many favorable merits including: (1) both the electrospinning and hydrothermal method have been proven to be a comparatively versatile, low cost, applicable and environmentally friendly technique. (2) This strategy can be extended to the fabrication of various hierarchical MOs, such as Co_3O_4, Fe_3O_4, Fe_2O_3, CuO, on TiO_2 nanofibers to form MOs/TiO_2 hierarchical heterostructures. (3) The synergistic effects of nanobuilding blocks as well as the unique hierarchical heterostructures may contribute to the improved LIBs performance. With this design, not only all the desired functions of each constituent are effectively utilized, but also a strong synergistic effect can be realized. As MOs feature both high capacity and higher electronic conductivity (compared to TiO_2), hierarchical heterostructures composed of TiO_2 nanofiber and various metal oxides (MOs) could simultaneously increase the rate capability and specific capacity of TiO_2 and improve the cycling performance of MOs by the synergistic effect. As a proof-of-concept demonstration of the application of such hierarchical heterostructures, the Co_3O_4/TiO_2 hierarchical heterostructures are tested as LIBs anode for the first time, which show high reversible capacity, improved cycling stability, and excellent rate capability with respect to the pristine TiO_2.

Results

Fabrication of MOs/TiO_2 hierarchical heterostructures. Four typical MOs, namely, Co_3O_4, Fe_2O_3, Fe_3O_4, and CuO, are adopted as secondary nanostructures grown on primary TiO_2 nanofiber to verify the feasibility and versatility of our protocol in achieving MO/TiO_2 hierarchical heterostructures. We firstly test this concept with Co_3O_4 nanosheets grown on primary TiO_2 nanofiber to form the Co_3O_4/TiO_2 hierarchical heterostructures. The morphology of the Co_3O_4/TiO_2 hierarchical heterostructures is investigated by scanning electron microscopy (SEM). As shown in Figure 1a, the obtained pristine TiO_2 non-woven nanofibers with diameters ranging from 200 to 500 nm have a relatively smooth surface without secondary nanostructures. After applying the controllable solution growth of Co_3O_4 nanosheets, the hierarchical heterostructures are formed (Figure 1b). Close observation on the nanofiber (Figure 1c) reveals that the high densities of secondary Co_3O_4 nanosheets grow on the primary TiO_2 nanofibers. Interestingly, compared with the hierarchical heterostructures before annealing treatment (Fig. S1a and b), it is obvious that many pores caused by the annealing treatment are found on the surface of the secondary Co_3O_4 nanosheets. These pores may exhibit large surface area, which is very

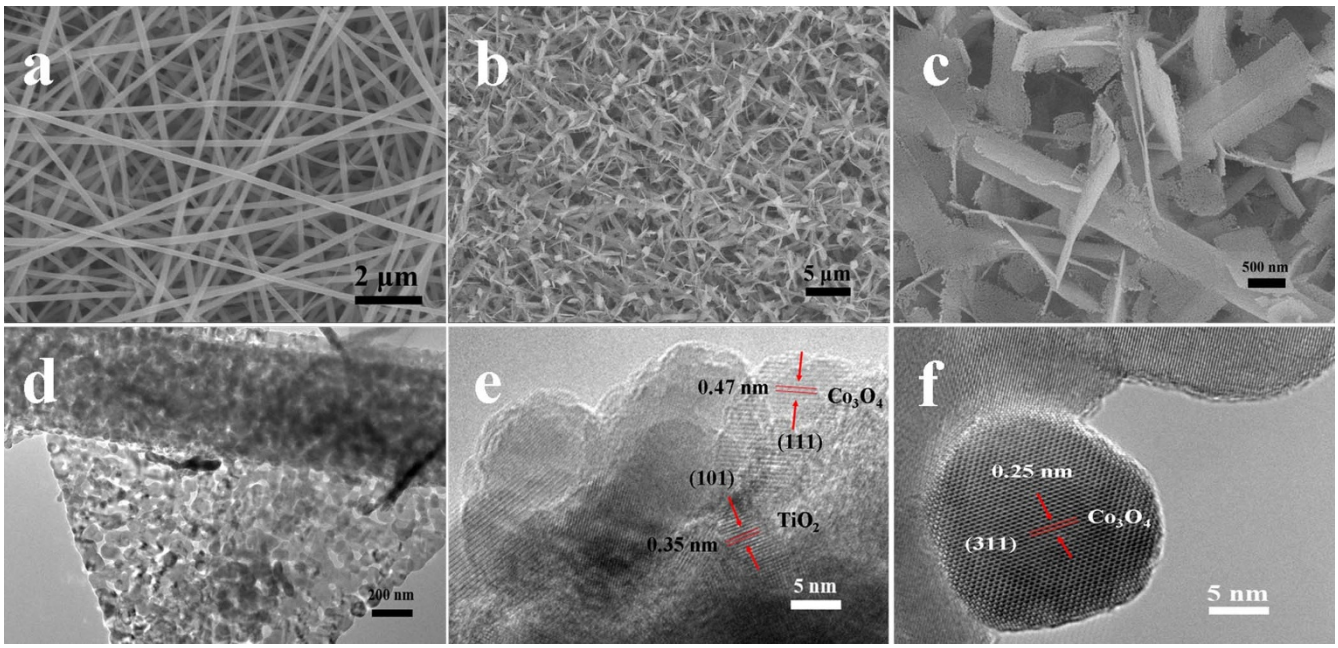

Figure 1 | Morphology characterization. (a) SEM image of pristine TiO_2 nanofibers. (b) Low- and (c) high-magnification SEM images of Co_3O_4/TiO_2 hierarchical heterostructures. (d) Typical TEM image of the single Co_3O_4/TiO_2 hierarchical nanofiber. (e) HRTEM image of the heterojunction region. (f) HRTEM image of the Co_3O_4 nanosheet surface.

precious for LIBs materials. Further information about the Co_3O_4/TiO_2 hierarchical heterostructures is obtained from transmission electron microscopy (TEM). The TEM image in Figure 1d shows an individual Co_3O_4/TiO_2 hierarchical nanofiber. It can be clearly seen that the secondary Co_3O_4 nanosheets with many pores grow on the surface of TiO_2 nanofibers, coinciding with the results from the SEM observations. The HRTEM image (Figure 1e) taken from the heterojunction region displays two set of lattice fringe spacings of 0.35 and 0.47 nm, corresponding to the (101) plane of the anatase crystal structure of TiO_2 and the (111) plane of the cubic Co_3O_4, respectively, which clearly shows the simultaneous presence of TiO_2 and Co_3O_4 crystal lattices in the region of the junction. Figure 1f shows the further magnified HRTEM image of the nanosheet, the measured lattice fringe spacings of 0.25 nm corresponding to the (311) plane of the cubic Co_3O_4 can be clearly observed.

To investigate the crystal phase of the samples, the X-ray diffraction (XRD) analysis is performed (Figure 2a). The XRD patterns reveal that all the diffraction peaks could be indexed to anatase TiO_2 (JCPDS No. 21–1272) and face-centered cubic phase of Co_3O_4 (space group: *Fd3m* (227), JCPDS No. 43-1003). These results confirm that the synthesis strategy adopted successfully achieves Co_3O_4/TiO_2 hierarchical heterostructures integrating the Co_3O_4 nanosheets and TiO_2 nanofibers. Subsequently, the purity, composition and fine structure of the samples are further investigated. In XPS spectra, Fig. S2 shows the characteristic peaks of C 1s, N 1s, O 1s, and Co 2p, respectively, indicating the existence of carbon, nitrogen, oxygen, and cobalt elements in the Co_3O_4/TiO_2 hierarchical heterostructures. The C 1s and N 1s peaks may be assigned to the pyrolysis of the urea. Obviously, the Ti signal is absent from this XPS spectra. As XPS is a highly surface-specific technique with a typical analysis depth of ~10 nm (lower than the thickness of the secondary Co_3O_4 shell), it is reasonable that TiO_2 is not detected[35]. This thus provides indirect experimental proof of the uniformity of the secondary Co_3O_4 nanostructures coating the TiO_2 nanofibers. In Raman spectra (Figure 2b), four well-resolved peaks are observed around 143.6 (E_g), 399.1 (B_{1g}), 519.3 (A_{1g}), and 639.7 (E_g) cm^{-1}, corresponding to the characteristic Raman modes of anatase TiO_2. After the growth of Co_3O_4 nanosheets, in addition to the peaks from anatase TiO_2, the new peaks at 193.6 (B_{1g}), 476.9 (E_g), 517.1 (F_{2g}), 615.1 (F_{2g}), 684.3 (A_{1g}) cm^{-1}, corresponding to the characteristic Raman modes of Co_3O_4, are observed and demonstrate the successful introduction of Co_3O_4. These results demonstrate the existence of both anatase TiO_2 and Co_3O_4 in the heterostructures.

The synthesis strategy can be readily extended to the growth of other MOs (e.g. Fe_2O_3, Fe_3O_4, and CuO) as secondary nanostructures on the primary TiO_2 nanofibers, forming MOs/TiO_2 hierarchical heterostructures. Similarly, the Fe_2O_3/TiO_2 hierarchical heterostructure can also be easily synthesized through our general strategy. The low- and high-magnification SEM images (Figure 3a and b) show the secondary Fe_2O_3 nanorods grown on the primary TiO_2 nanofibers to form Fe_2O_3/TiO_2 hierarchical heterostructures with diameters of about 290 nm. The structure is further investigated by TEM in more detail. Figure 3c shows that Fe_2O_3 nanorods are uniformly attached on the primary TiO_2 nanofibers surface, and the selected circular area is enlarged (Figure 3c, inset). The diameter and length of Fe_2O_3 nanorods are estimated to be about 22 and 45 nm, respectively. The HRTEM image (Figure 3d) further confirms the single-crystalline structure of the α-Fe_2O_3 nanorods with a lattice fringe spacing of 0.37 nm from the (311) plane.

Apart from Co_3O_4 and Fe_2O_3, Fe_3O_4 and CuO nanoparticles grown on the primary TiO_2 nanofibers are employed to further demonstrate the efficiency and generality of our strategy. The resulting composites exhibit the hierarchical nanostructure with secondary nanoparticles grown on the major nanofibers (Figure 4). In the case of Fe_3O_4/TiO_2 hierarchical heterostructures, the secondary Fe_3O_4 nanoparticles with diameters of about 40 nm are grown on the TiO_2 nanofiber substrates. In the case of CuO/TiO_2 hierarchical heterostructures, the secondary CuO nanoparticles with diameters of about 600 nm are grown on the TiO_2 nanofiber substrates. Furthermore, the crystal structure information and the chemical components of the heterostructure are characterized by XRD (Figure 5). Their XRD peaks can be well indexed as rhombohedral hematite α-Fe_2O_3 (JCPDS No. 33-0664), cubic magnetite Fe_3O_4 (JCPDS No. 19-0629) and tenorite CuO (JCPDS No. 48-1548), respectively. Strong and sharp diffraction peaks of the patterns suggest that the as-synthesized hierarchical heterostructures are highly crystallized.

Formation mechanism of Co_3O_4/TiO_2 hierarchical heterostructures. Based on the above analysis, combining the versatility of the electrospinning technique and hydrothermal growth enables the fabrication of MO/TiO_2 hierarchical heterostructures. Evidently, no surface pretreatments are needed to introduce new surface functional groups or additional covalent and/or noncovalent interconnectivity in our experiments. Subsequently, we take Co_3O_4/TiO_2 hierarchical heterostructures as an example and investigate the formation mechanism of hierarchical heterostructures, as illustrated in Figure 6.

To get more insight into the actual evolution process of the Co_3O_4/TiO_2 hierarchical heterostructures, a series of time-dependent experiments is conducted, and the intermediate solids at the different reaction stages (nucleation, growth, etc.) are examined. Figure 6a-f show representative SEM images for the samples collected stepwise

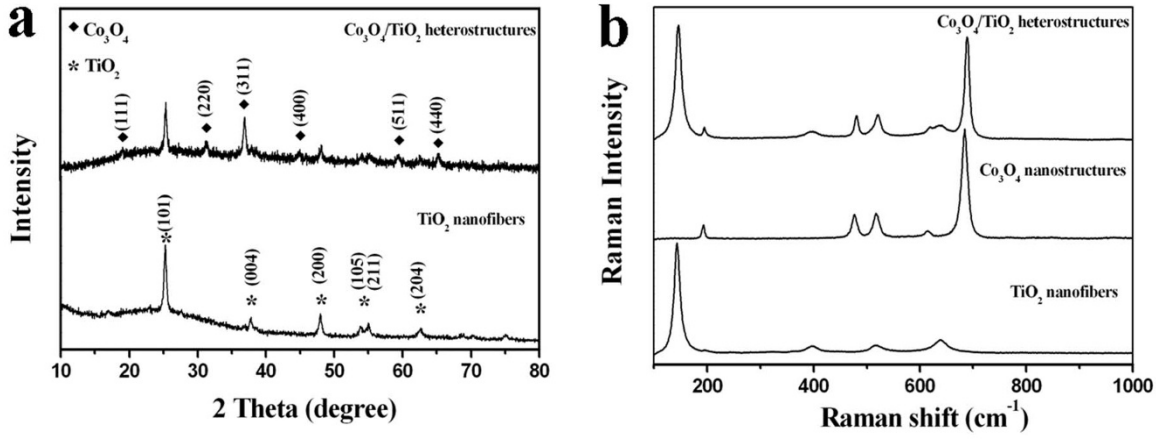

Figure 2 | Phase analysis. (a) XRD patterns of pristine TiO_2 nanofibers and Co_3O_4/TiO_2 hierarchical heterostructures. (b) Raman spectra of pristine TiO_2 nanofibers, Co_3O_4 nanostructures, and Co_3O_4/TiO_2 hierarchical heterostructures.

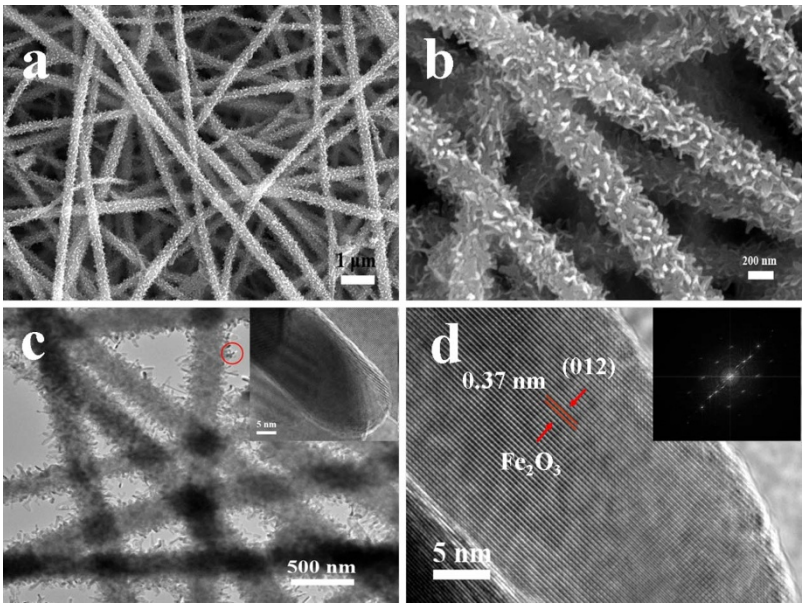

Figure 3 | Morphology characterization. (a) Low- and (b) high-magnification SEM images of Fe_2O_3/TiO_2 hierarchical heterostructures. (c) Low- and high-magnification (inset) TEM images of Fe_2O_3/TiO_2 hierarchical heterostructures. (d) HRTEM image and fast-Fourier transformation (FFT) of the Fe_2O_3 nanorod surface.

after 1, 1.5, 2, 4, 6, and 9 h of reaction. These sequential images reveal a morphological and structural transformation from pristine TiO_2 nanofibers to Co_3O_4/TiO_2 hierarchical nanofibers. Evidently, in the initial stage (1 h) of the hydrothermal reaction, there is no visible change to the pristine TiO_2 nanofibers (Figure 6a). However, after 1.5 h growth, tiny nanowires nucleated on the surfaces of the TiO_2 nanofibers are observed (Figure 6b). When the reaction time is extended to 2 h, although a few nanosheets have already formed, most TiO_2 nanofibers appeared to be surrounded by tiny nanowires (Figure 6c). When the reaction time is further extended to 4 h, the continuous growth results in the disappearance of the tiny nanowires. As a result, the secondary nanosheets grow on the primary TiO_2 nanofibers (Figure 6d). However, by further increasing the reaction time, the overall morphology scarcely shows any change (Figure 6e and f).

Based on the time-dependent experiments, the possible mechanism is proposed to explain the formation of these hierarchical heterostructures (Figure 6g). Firstly, the electrospun TiO_2 nanofibers provide negative charges on the surface, which is demonstrated by its negative zeta potential (−29.4 mV). It is well known that when two components with opposite charges are carefully introduced together, the mutual electrostatic interactions drive Co^{2+} to attach on the surfaces of the TiO_2 nanofibers. Then, the reaction of Co^{2+} and urea takes place and the formed cobalt-hydroxide-carbonate nuclei attach

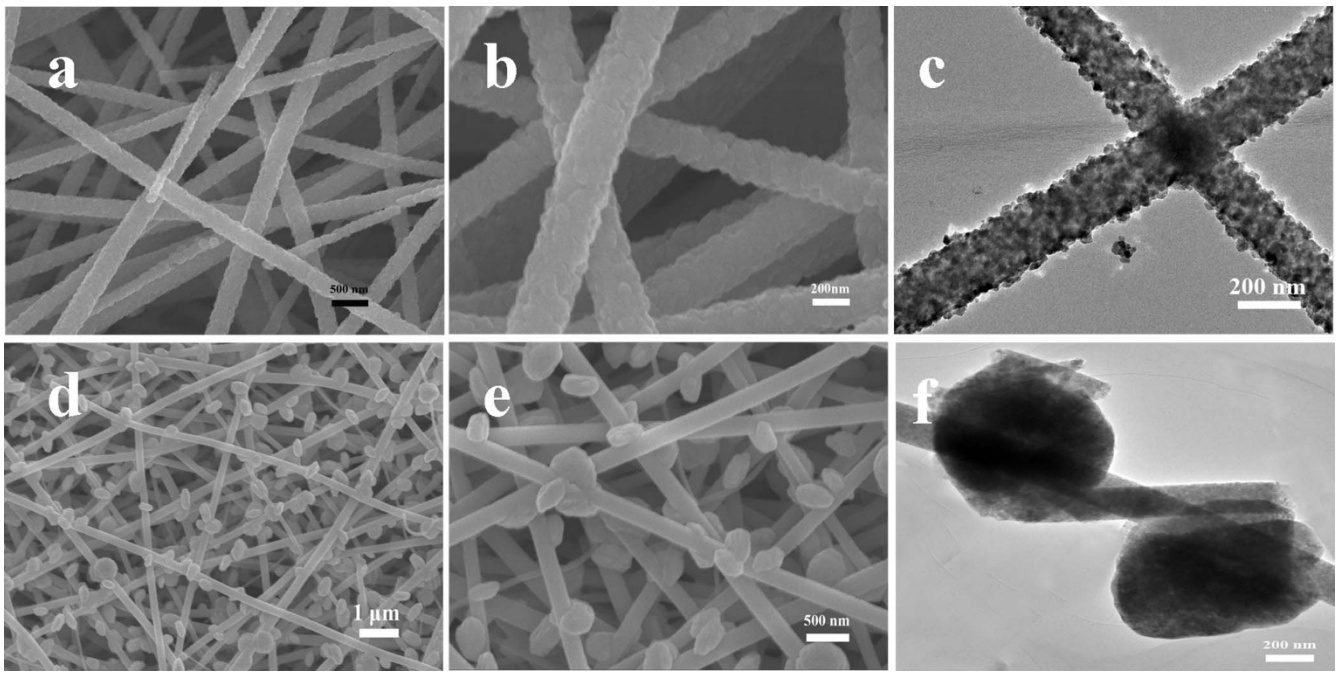

Figure 4 | Morphology characterization. (a) Low-magnification, (b) high-magnification SEM images and (c) TEM image of Fe_3O_4/TiO_2 hierarchical heterostructures. (d) Low-magnification, (e) high-magnification SEM images and (f) TEM image of CuO/TiO_2 hierarchical heterostructures.

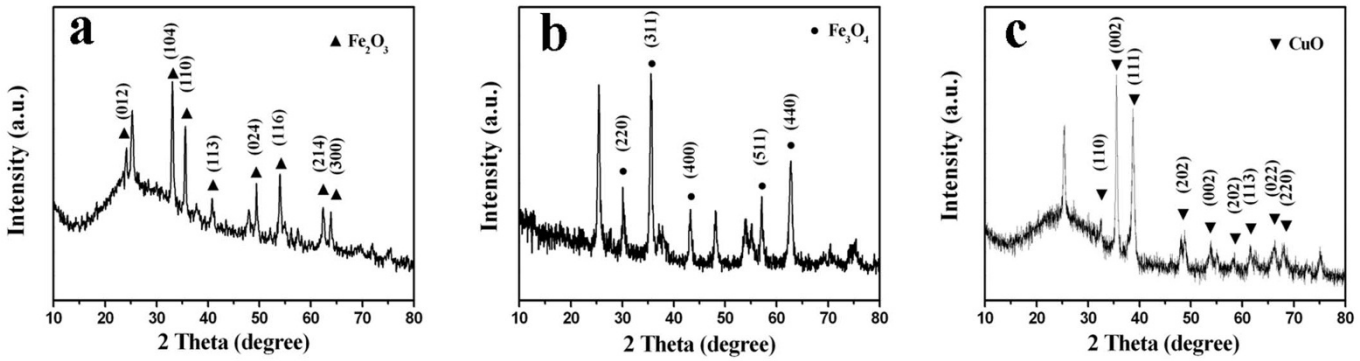

Figure 5 | Phase analysis. XRD patterns of (a) Fe_2O_3/TiO_2, (b) Fe_3O_4/TiO_2, and (c) CuO/TiO_2 hierarchical heterostructures.

to the surface of pristine TiO_2 nanofibers. In the reaction, TiO_2 nanofibers are used as the substrate, which can guide the secondary nanoparticles self-assembling growth in aqueous solution without surfactant and stabilizers. In this key step, the uniform small nuclei are very important because they could determine the growth kinetics of the nanosheets on the surface of the TiO_2 nanofibers[36]. Then the oriented attachment can guide the nanoparticles growth[37]. With the continuously reaction proceeding, the precursors are consumed for the oriented growth to form large-scale nanosheets surrounding the TiO_2 nanofibers. With our starting chemical precursors, the formation of the cobalt-hydroxide-carbonate phase can be demonstrated by the XRD patterns (Fig. S3), which agrees well with previous reports[38,39]. Finally, the cobalt-hydroxide-carbonate transforms into Co_3O_4 induced by the thermal annealing. Upon annealing for 4 h in air, cobalt-hydroxide-carbonate decomposes gradually and black Co_3O_4 nanosheets are obtained accordingly. Obviously, large quantities of pores are widely distributed on the surface of Co_3O_4 nanosheets, the yield of which would mainly rely on the pyrolysis of hydroxide-carbonate and the release of gases (CO_2, H_2O) during the calcination process[40].

Electrochemical performance of Co_3O_4/TiO_2 hierarchical heterostructures. To demonstrate the effectiveness of the TiO_2-based hierarchical nanofibers in improving the lithium storage performance, we take Co_3O_4/TiO_2 hierarchical heterostructures as a representative example and investigate the electrochemical properties of them as anode materials for LIBs, since Co_3O_4 has high theoretical capacity (~890 mA h g^{-1}), and is widely considered to be an attractive anode material for next-generation LIBs.

Figure 7a shows the representative cyclic voltammetry (CV) curves of the Co_3O_4/TiO_2 hierarchical heterostructures in the voltage range of 0.01–3 V. Evidently, a pronounced reduction/oxidation peak appeared at 1.7/2.1 V is as the same as that reported for anatase TiO_2, characteristic for the lithium storage mechanism between tetragonal anatase and orthorhombic Li_xTiO_2 ($TiO_2 + xLi^+ + xe^- \leftrightarrow Li_xTiO_2$)[2,41,42]. In addition, the reduction peak at ~0.98 V and ~0.66 V during the cathodic process in the first cycle can be ascribed to the initial reduction of Co_3O_4 to Co, the electrochemical formation of amorphous Li_2O, and the formation of a partially irreversible solid electrolyte interphase (SEI) layer[32–34]. It is noted that reversible formation could be electrochemically driven by the metal

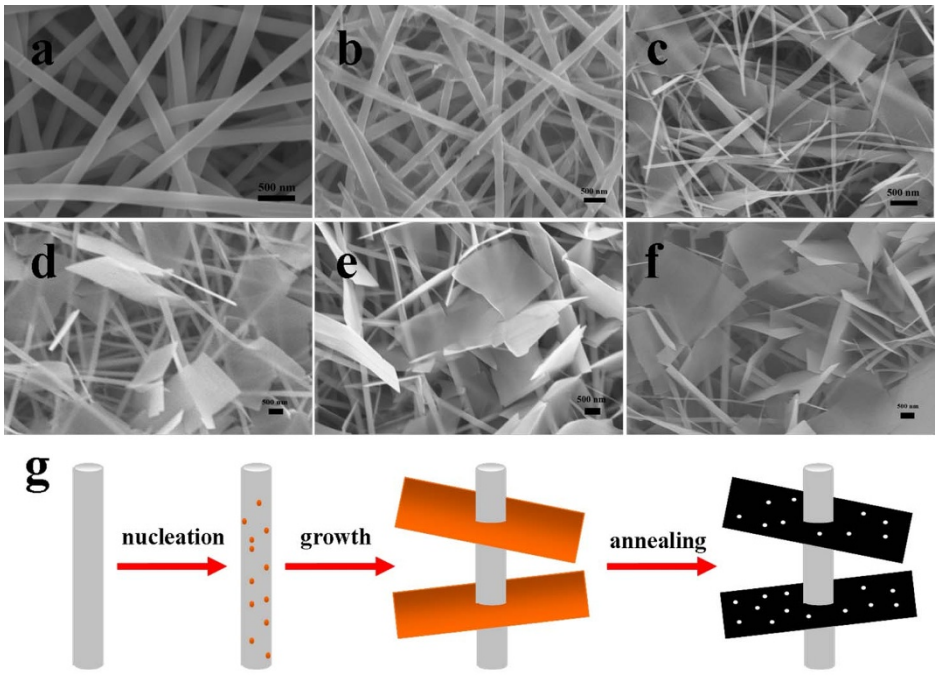

Figure 6 | Formation mechanism of Co_3O_4/TiO_2 hierarchical heterostructures. SEM images of Co_3O_4/TiO_2 hierarchical heterostructures (before annealing) at various reaction stages by setting the reaction time 1 h (a), 1.5 h (b), 2 h (c), 4 h (d), 6 h (e), and 9 h (f). And schematic of the formation process of Co_3O_4/TiO_2 hierarchical heterostructures (g).

nanoparticles formed in situ. Hence, the presence of Co nanoparticles at the interface between TiO_2 and Co_3O_4 may improve the reversibility reaction of the anatase TiO_2 and further result in a reversible capacity[5]. In general, during the anodic process, the oxidation of metallic Co to Co_3O_4 and the decomposition of Li_2O could result in the appearance of the oxidation peak at ~2.1 V[32–34]. Interestingly, in present case, only one oxidation peak at about 2.1 V is observed, it is obvious that these two oxidation peaks coincide with each other. Note that, the second and onward CV curves remain steady, indicating the excellent cycle stability of the hierarchical heterostructures. Subsequently, the lithium storage performance of the Co_3O_4/TiO_2 hierarchical heterostructures is investigated. Figure 7b shows the discharge and charge curves at a current density of 200 mA g^{-1}. Consistent with the above CV analysis, the similar current peaks can be identified. These voltage profiles are characteristic of both Co_3O_4-based and TiO_2-based materials. It is observed that the initial discharge and charge capacities of the Co_3O_4/TiO_2 hierarchical heterostructures electrode are 632.5 and 499.7 mAh g^{-1}, respectively, corresponding to an irreversible capacity loss of 21.0%. The capacity of the Co_3O_4/TiO_2 hierarchical heterostructures electrode does not decay, and it can deliver a reversible capacity of 602.8 mAh g^{-1} even after 480 cycles (Figure 7b and c). Importantly, the Co_3O_4/TiO_2 hierarchical heterostructures electrode still exhibits an excellent cyclic performance at a higher current density of 500 mA g^{-1}, and the capacity still reaches 302.9 mA g^{-1} after 250 discharge and charge cycles (Fig. S4). In contrast, the pristine TiO_2 nanofibers electrode only exhibits a very lower capacity (initial discharge and charge capacities of 275.8 and 159.8 mAh g^{-1}), and the single Co_3O_4 nanostructures electrode loses the capacity severely (the discharge capacity of 381.4 mAh g^{-1} after only 90 charge-discharge cycles) (Fig. S5). Evidently, the composite hierarchical heterostructures inherit the advantages of high capacity from Co_3O_4 component and the excellent stability of TiO_2 component. To better understand the advantage of the hierarchical heterostructures in lithium storage, the rate performance of the Co_3O_4/TiO_2 hierarchical heterostructures is investigated (Figure 7d). Obviously, compared with the pristine TiO_2 nanofibers, the specific capacity of the hierarchical heterostructures is substantially increased at all investigated charge-discharge rates from 100 to 2000 mA g^{-1}. For example, the Co_3O_4/TiO_2 hierarchical heterostructures exhibit much superior rate performance with 475.8 and 449.5 mAh g^{-1}, which is about three times larger than that of pristine TiO_2 electrode (143.2 and 115.3 mAh g^{-1}), at current densities of 400 and 1000 mA g^{-1}, respectively. At the high current rate (2000 mA g^{-1}), the hierarchical heterostructures exhibit a downward trend, which can be ascribed to the partial collapse of the electrode materials during the charge–discharge at a high current density. Further investigations are ongoing to improve the capacity retention at high discharge rates. However, the difference of rate performance between the two materials is quite more remarkable even at high current density. Importantly, the high capacity of the hierarchical composite electrode can be recovered to the initial values even after 70 discharge and charge cycles, implying their good reversibility.

Discussion

The above obtained improved electrochemical properties of the Co_3O_4/TiO_2 hierarchical heterostructures are not simply a result of the mix of the two components. Instead, it more likely originates

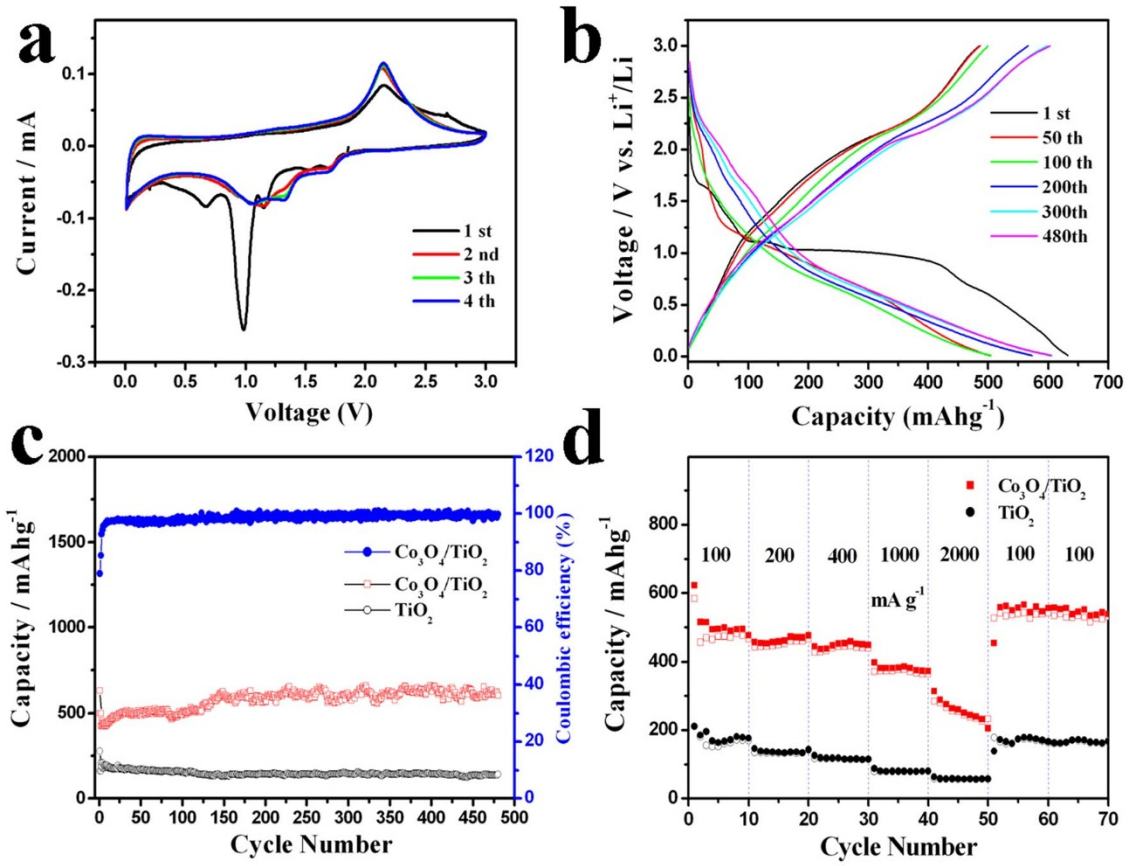

Figure 7 | Electrochemical properties of Co_3O_4/TiO_2 hierarchical heterostructures. (a) CV of Co_3O_4/TiO_2 hierarchical heterostructures at a scan rate of 0.1 mV s^{-1} in the range of 3–0.01 V. (b) Discharge and charge curves of Co_3O_4/TiO_2 hierarchical heterostructures at a current density of 200 mA g^{-1} in the range of 3–0.01 V. (c) Cycling performance and coulombic efficiency of pristine TiO_2 nanofibers and Co_3O_4/TiO_2 hierarchical heterostructures at a current density of 200 mA g^{-1}. (d) Rate performance of pristine TiO_2 nanofibers and Co_3O_4/TiO_2 hierarchical heterostructures.

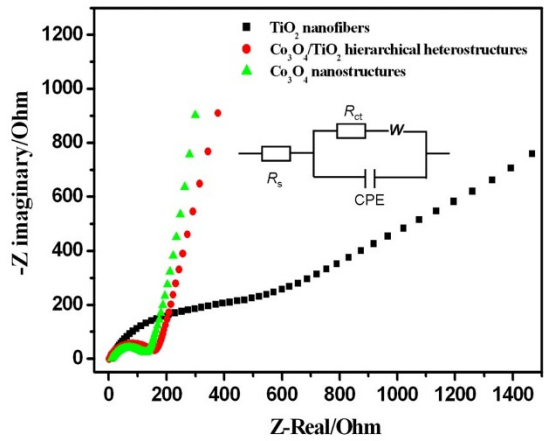

Figure 8 | Electrochemical impedance spectra of Co_3O_4/TiO_2 hierarchical heterostructures. Nyquist plots before cycling for the pristine TiO_2 nanofibers, single Co_3O_4 nanostructures and Co_3O_4/TiO_2 hierarchical heterostructures by applying an AC voltage of 5 mV amplitude at 0.1 Hz to 700 kHz.

from the successful integration of the respective advantages from both TiO_2 and Co_3O_4 individual components into the unique hierarchical heterostructures, which is elaborated as follows. On one hand, the improved capacity of hierarchical heterostructures compared with the pristine TiO_2 nanofibers can be easily understood by the addition of a higher capacity Co_3O_4 component and the synergistic effect of Co_3O_4 nanosheets and TiO_2 stems mentioned above. It is well-known that one advantage of transition-metal oxides in lithium storage is their high theoretical specific capacity. Hence, a large content of Co_3O_4 could give rise to a high specific capacity. On the other hand, the synergistic effect of the successful integration of the Co_3O_4 nanosheets and TiO_2 nanofibers contributes more to the improved cycling stability and excellent rate capability of the Co_3O_4/TiO_2 hierarchical heterostructures. Herein, the reason can be the following: the Co_3O_4 nanosheets with many spaces each other have an increased portion of exposed surfaces and ensure a high utilization of electrode materials, thus a high capacity. Besides, the ultralong hierarchical heterostructures can suppress the self-aggregation, buffer the volume changes of Co_3O_4 nanosheets, and keep the effective contact areas of active materials and electrolyte large and sufficient during the cycling, thereby resulting in better cyclic stability[5,43]. Specifically, in comparison with the pristine TiO_2 nanofibers, the highly dense Co_3O_4 nanosheets grow on the TiO_2 nanofibers substrate orderly. This structure can provide more electrochemically active sites and sufficient order to enable Li^+ access to the heterostructures facilely. In addition to the improved cycling stability, the Co_3O_4/TiO_2 hierarchical heterostructures also exhibit excellent rate capability with respect to the pristine TiO_2 nanofibers. Therefore, the difference in the conductivity between them should be taken into account. To probe the kinetic properties of the hierarchical heterostructures, we take the electrochemical impedance spectroscopy (EIS) measurements. All three plots show partially overlapping semicircles at high-to-medium frequencies, and a line was observed at low frequencies in Figure 8. Apparently, the charge transfer resistances R_{ct} for the three samples is in the ascending order of TiO_2 (730.0 Ω) > Co_3O_4/TiO_2 (170.9 Ω) > Co_3O_4 (137.2 Ω), whilst the contact resistances (see the intercept of the real axis in Figure 8) between electrolyte and electrode materials are similar, which indicates that the secondary Co_3O_4 nanosheets coating could enable much easier charge transfer at the electrode/electrolyte interface (compared with TiO_2 nanofibers) and boost the electronic conductivity. Thus, the improved electronic conductivity is considered to be a key factor in improving the rate capability and cyclic life of the Co_3O_4/TiO_2 hierarchical heterostructures.

In summary, a simple, general yet effective strategy is developed based on the advantageously combination of the versatility of the electrospinning technique and hydrothermal growth to achieve various MOs, including Co_3O_4, Fe_2O_3, Fe_3O_4, and CuO, grown on pristine TiO_2 nanofibers to form MO/TiO_2 hierarchical heterostructures. As potential anode materials for LIBs, the as-formed Co_3O_4/TiO_2 hierarchical heterostructures exhibit high reversible capacity, improved cycling stability and rate capability with respect to the pristine TiO_2 nanofibers. The improved electrochemical performance is ascribed to the synergistic effect of the advantageous integration of Co_3O_4 and TiO_2 hierarchical nanostructure. The proposed synthesis strategy would open up new opportunities in the development of high performance next-generation LIBs used for alternative energy and electric transportation. Such hierarchical heterostructures might also be used in broad fields including photoelectrochemical water splitting and gas sensors.

Methods

Sample synthesis. The MO/TiO_2 hierarchical nanostructures were prepared by the electrospinning and hydrothermal method[44]. Typically, 0.2429 g $Co(NO_3)_2 \cdot 6H_2O$ and 0.25 g urea were dissolved in 25 mL deionized water under magnetic stirring. Then the resulting solution was transferred into a 50 mL Teflon-lined autoclave with electrospun TiO_2 nanofibers (20 mg). The autoclave was sealed and heated at 120°C for 6 h, and cooled to room temperature. The film was collected out, washed with ethanol and deionized water, respectively, and then dried under vacuum at 50°C for 12 h. Then the as-collected films were calcined at 400°C for 4 h. For comparison, the single Co_3O_4 nanostructures were also prepared under the same condition instead of the addition of TiO_2 nanofibers. When Co_3O_4 precursor solution was replaced by Fe_2O_3 precursor solution (0.243 g $FeCl_3$ and 30 mL deionized water), Fe_3O_4 precursor solution (0.25 g $FeCl_3 \cdot 6H_2O$, 0.25 g polyethylene glycol, 0.9 g sodium acetate and 25 mL ethylene glycol), and CuO precursor solution (0.2557 g $CuCl_2 \cdot 2H_2O$, 0.3 g urea and 30 mL deionized water), and the autoclave was sealed and heated at 90°C for 6 h (Fe_2O_3), at 200°C for 16 h (Fe_3O_4), or at 180°C for 12 h (CuO), then the as-collected films were calcined at 500°C for 2 h except Fe_3O_4/TiO_2 hierarchical nanofibers.

Sample characterization. The morphology and crystalline structure of as-obtained samples were characterized with scanning electron microscopy (SEM Hitachi S-4800) and transmission electron microscope (TEM) recorded on a Tecnai G2 operating at 200 kV. X-ray diffraction (XRD) patterns were recorded on a Rigaku-Dmax 2500 diffractometer with Cu Kα radiation. X-ray photoelectron spectroscopy (XPS) analysis was carried on an ESCALAB MK X-ray photoelectron spectrometer. Zeta potential was measured by dynamic light scattering (Malvern Nano-ZS). Raman measurements were performed at room temperature using an inVia Reflex Raman spectrometer with Raman shift from 100 to 1000 cm^{-1}.

Electrochemical evaluation. The electrodes were prepared by mixing active materials (70 wt%), acetylene black (20 wt%), and polyvinylidene fluoride (PVDF, 10 wt%) in N-methyl-2-pyrrolidone (NMP). After the above slurries were uniformly spread onto a copper foil, the electrodes were dried at 80°C in vacuum for 6 h. Then the electrodes were pressed and cut into disks before transferring into an Argon-filled glove box. Coin cells (CR2025) were laboratory-assembled using lithium metal as the counter electrode, Celgard 2400 membrane as the separator and $LiPF_6$ (1 M) in ethylene carbonate/dimethyl carbonate (EC/DMC, 1:1 vol%) as the electrolyte. The galvanostatic charge-discharge tests were carried out on a Land Battery Measurement System (Land, China). Cyclic voltammetry (CV) and impedance were performed using a VMP3 Electrochemical Workstation (Bio-logic Inc.).

1. Magasinski, A. *et al.* High-Performance Lithium-Ion Anodes Using a Hierarchical Bottom-Up Approach. *Nat. Mater.* **9**, 353–358 (2010).
2. Chen, J. S. *et al.* Constructing Hierarchical Spheres from Large Ultrathin Anatase TiO_2 Nanosheets with Nearly 100% Exposed (001) Facets for Fast Reversible Lithium Storage. *J. Am. Chem. Soc.* **132**, 6124–6130 (2010).
3. Sun, Y. M. *et al.* Self-Assembled Hierarchical MoO_2/Graphene Nanoarchitectures and Their Application as a High-Performance Anode Material for Lithium-Ion Batteries. *ACS Nano* **5**, 7100–7107 (2011).
4. Sun, Y. M. *et al.* Morphosynthesis of a Hierarchical MoO_2 Nanoarchitecture as a Binder-Free Anode for Lithium-Ion Batteries. *Energy Environ. Sci.* **4**, 2870–2877 (2011).
5. Zhou, W. W. *et al.* Epitaxial Growth of Branched α-Fe_2O_3/SnO_2 Nano-Heterostructures with Improved Lithium-Ion Battery Performance. *Adv. Funct. Mater.* **21**, 2439–2445 (2011).
6. Yan, J., Sumboja, A., Khoo, E. & Lee, P. S. V_2O_5 Loaded on SnO_2 Nanowires for High-Rate Li Ion Batteries. *Adv. Mater.* **23**, 746–750 (2011).
7. Gratzel, M. Photoelectrochemical Cells. *Nature* **414**, 338–344 (2001).
8. Bruce, P. G., Scrosati, B. & Tarascon, J. M. Nanomaterials for Rechargeable Lithium Batteries. *Angew. Chem. Int. Ed.* **47**, 2930–2946 (2008).

9. Zhu, H. Y. *et al.* Phase Transition between Nanostructures of Titanate and Titanium Dioxides via Simple Wet-Chemical Reactions. *J. Am. Chem. Soc.* **127**, 6730–6736 (2005).
10. Lee, K. *et al.* Anodic Formation of Thick Anatase TiO_2 Mesosponge Layers for High-Efficiency Photocatalysis. *J. Am. Chem. Soc.* **132**, 1478–1479 (2010).
11. Cho, C. Y. & Moon, J. H. Hierarchically Porous TiO_2 Electrodes Fabricated by Dual Templating Methods for Dye-Sensitized Solar Cells. *Adv. Mater.* **23**, 2971–2975 (2011).
12. Liu, J. H. *et al.* Sandwich-Like, Stacked Ultrathin Titanate Nanosheets for Ultrafast Lithium Storage. *Adv. Mater.* **23**, 998–1002 (2011).
13. Chen, J. S., Liu, H., Qiao, S. Z. & Lou, X. W. Carbon-Supported Ultra-Thin Anatase TiO_2 Nanosheets for Fast Reversible Lithium Storage. *J. Mater. Chem.* **21**, 5687–5692 (2011).
14. Armstrong, A. R. *et al.* Lithium-Ion Intercalation into TiO_2-B Nanowires. *Adv. Mater.* **17**, 862–865 (2005).
15. Wagemaker, M., Borghols, W. J. H. & Mulder, F. M. Large Impact of Particle Size on Insertion Reactions. A Case for Anatase Li_xTiO_2. *J. Am. Chem. Soc.* **129**, 4323–4327 (2007).
16. Chen, X. & Mao, S. S. Titanium Dioxide Nanomaterials: Synthesis, Properties, Modifications, and Applications. *Chem. Rev.* **107**, 2891–2959 (2007).
17. Rahman, M. M. *et al.* Amorphous Carbon Coated High Grain Boundary Density Dual Phase $Li_4Ti_5O_{12}$-TiO_2: A Nanocomposite Anode Material for Li-Ion Batteries. *Adv. Energy Mater.* **1**, 212–220 (2011).
18. Myung, S. T. *et al.* Nanostructured TiO_2 and Its Application in Lithium-Ion Storage. *Adv. Funct. Mater.* **21**, 3231–3241 (2011).
19. Armstrong, G. *et al.* TiO_2(B) Nanowires as an Improved Anode Material for Lithium-Ion Batteries Containing $LiFePO_4$ or $LiNi_{0.5}Mn_{1.5}O_4$ Cathodes and a Polymer Electrolyte. *Adv. Mater.* **18**, 2597–2600 (2006).
20. Han, H. *et al.* Nitridated TiO_2 Hollow Nanofibers as an Anode Material for High Power Lithium Ion Batteries. *Energy Environ. Sci.* **4**, 4532–4536 (2011).
21. Yuan, T. *et al.* Electrospinning Based Fabrication and Performance Improvement of Film Electrodes for Lithium-Ion Batteries Composed of TiO_2 Hollow Fibers. *J. Mater. Chem.* **21**, 15041–15048 (2011).
22. Moriguchi, I. *et al.* Mesoporous Nanocomposite of TiO_2 and Carbon Nanotubes as a High-Rate Li-Intercalation Electrode Material. *Adv. Mater.* **18**, 69–73 (2006).
23. Yang, S. B., Feng, X. L. & Müllen, K. Sandwich-Like, Graphene-Based Titania Nanosheets with High Surface Area for Fast Lithium Storage. *Adv. Mater.* **23**, 3575–3579 (2011).
24. Li, N. *et al.* Battery Performance and Photocatalytic Activity of Mesoporous Anatase TiO_2 Nanospheres/Graphene Composites by Template-Free Self-Assembly. *Adv. Funct. Mater.* **21**, 1717–1722 (2011).
25. Nam, S. H. *et al.* Ag or Au Nanoparticle-Embedded One-Dimensional Composite TiO_2 Nanofibers Prepared via Electrospinning for Use in Lithium-Ion Batteries. *ACS Appl. Mater. Interface* **2**, 2046–2052 (2010).
26. He, B. L., Dong, B. & Li, H. L. Preparation and Electrochemical Properties of Ag-Modified TiO_2 Nanotube Anode Material for Lithium–Ion Battery. *Electrochem. Commun.* **9**, 425–430 (2007).
27. Guo, Y. G., Hu, Y. S., Sigle, W. & Maier, J. Superior Electrode Performance of Nanostructured Mesoporous TiO_2 (Anatase) through Efficient Hierarchical Mixed Conducting Networks. *Adv. Mater.* **19**, 2087–2091 (2007).
28. Dong, S. *et al.* One Dimensional MnO_2/Titanium Nitride Nanotube Coaxial Arrays for High Performance Electrochemical Capacitive Energy Storage. *Energy Environ. Sci.* **4**, 3502–3508 (2011).
29. Poizot, P. *et al.* Nano-Sized Transition-Metal Oxides as Negative-Electrode Materials for Lithium-Ion Batteries. *Nature* **407**, 496–499 (2000).
30. Mitra, S., Poizot, P., Finke, A. & Tarascon, J. M. Growth and Electrochemical Characterization versus Lithium of Fe_3O_4 Electrodes Made via Electrodeposition. *Adv. Funct. Mater.* **16**, 2281–2287 (2006).
31. Yang, S. B. *et al.* Porous Iron Oxide Ribbons Grown on Graphene for High-Performance Lithium Storage. *Sci. Rep.* **2**, 427 (2012).
32. Wang, Y., Xia, H., Lu, L. & Lin, J. Y. Excellent Performance in Lithium-Ion Battery Anodes: Rational Synthesis of $Co(CO_3)_{0.5}(OH)0.11H_2O$ Nanobelt Array and Its Conversion into Mesoporous and Single-Crystal Co_3O_4. *ACS Nano* **4**, 1425–1432 (2010).
33. Xiong, S. L., Chen, J. S., Lou, X. W. & Zeng, H. C. Mesoporous Co_3O_4 and CoO@C Topotactically Transformed from Chrysanthemum-like $Co(CO_3)_{0.5}(OH)\cdot 0.11H_2O$ and Their Lithium-Storage Properties *Adv. Funct. Mater.* **22**, 861–871 (2012).
34. Li, W. Y., Xu, L. N. & Chen, J. Co_3O_4 Nanomaterials in Lithium-Ion Batteries and Gas Sensors. *Adv. Funct. Mater.* **15**, 851–857 (2005).
35. Xuan S. H., Jiang W. Q., Gong X. L., Hu Y. & Chen Z. Y. Magnetically Separable Fe_3O_4/TiO_2 Hollow Spheres: Fabrication and Photocatalytic Activity. *J. Phys. Chem. C* **113**, 553–558 (2009).
36. Shang, M. *et al.* General Strategy for a Large-Scale Fabric with Branched Nanofiber–Nanorod Hierarchical Heterostructure: Controllable Synthesis and Applications. *Chem. Eur. J* **16**, 11412–11419 (2010).
37. Mai, L. Q. *et al.* Hierarchical $MnMoO_4$/$CoMoO_4$ Heterostructured Nanowires with Enhanced Supercapacitor Performance. *Nat. Commun.* **2**, 318 (2011).
38. Jiang, J. *et al.* General Synthesis of Large-Scale Arrays of One-Dimensional Nanostructured Co_3O_4 Directly on Heterogeneous Substrates. *Cryst. Growth Des.* **10**, 70–75 (2010).
39. Xu, R. & Zeng, H. C. Dimensional Control of Cobalt-hydroxide-carbonate Nanorods and Their Thermal Conversion to One-Dimensional Arrays of Co_3O_4 Nanoparticles. *J. Phys. Chem. B* **107**, 12643–12649 (2003).
40. Jiang, J. *et al.* Direct Synthesis of CoO Porous Nanowire Arrays on Ti Substrate and Their Application as Lithium-Ion Battery Electrodes. *J. Phys. Chem. C* **114**, 929–932 (2010).
41. Lou, X. W. & Archer, L. A. A General Route to Nonspherical Anatase TiO_2 Hollow Colloids and Magnetic Multifunctional Particles. *Adv. Mater.* **20**, 1853–1858 (2008).
42. Kim, S. W. *et al.* Fabrication and Electrochemical Characterization of TiO_2 Three-Dimensional Nanonetwork Based on Peptide Assembly. *ACS Nano* **3**, 1085–1090 (2009).
43. Mai, L. *et al.* Electrospun Ultralong Hierarchical Vanadium Oxide Nanowires with High Performance for Lithium Ion Batteries. *Nano Lett.* **10**, 4750–4755 (2010).
44. Wang, H. G. *et al.* Magnetically Separable Iron Oxide Nanostructures-TiO_2 Nanofibers Hierarchical Heterostructures: Controlled Fabrication and Photocatalytic Activity. *New J. Chem.* **35**, 1795–1802 (2011).

Acknowledgments

This work is financially supported by 100 Talents Programme of The Chinese Academy of Sciences, National Program on Key Basic Research Project of China (973 Program, Grant No. 2012CB215500), Foundation for Innovative Research Groups of the National Natural Science Foundation of China (Grant No. 20921002), National Natural Science Foundation of China (Grant No. 21101147), and the Jilin Province Science and Technology Development Program (Grant No. 20100102 and 20116008).

Author contributions

H.G.W. carried out the experiments and wrote the paper. D.L.M., Y.H. and X.L.H. conducted the SEM and TEM measurements. X.B.Z. supervised the research and revised the manuscript. All authors reviewed the manuscript.

Additional information

Supplementary information accompanies this paper at http://www.nature.com/scientificreports

Competing financial interests: The authors declare no competing financial interests.

How to cite this article: Wang, H., Ma, D., Huang, X., Huang, Y. & Zhang, X. General and Controllable Synthesis Strategy of Metal Oxide/TiO_2 Hierarchical Heterostructures with Improved Lithium-Ion Battery Performance. *Sci. Rep.* **2**, 701; DOI:10.1038/srep00701 (2012).